Journal of Nuclear Materials 455 (2014) 710–716

Contents lists available at ScienceDirect

Journal of Nuclear Materials

journal homepage: www.elsevier.com/locate/jnucmat

Overview of plasma–material interaction experiments on EAST employing MAPES

Fang Ding [a], Guang-Nan Luo [a,*], Richard A. Pitts [b], Andrey Litnovsky [c], Xianzu Gong [a], Rui Ding [a], Hongmin Mao [a], Haishan Zhou [a,f], William R. Wampler [d], Peter C. Stangeby [e], Sophie Carpentier [b], Maren Hellwig [c], Rong Yan [a], Naoko Ashikawa [f], Masakatsu Fukumoto [g], Kazunari Katayama [h], Wenzhang Wang [a], Huiqian Wang [a], Liang Chen [a], Jing Wu [a], Junling Chen [a], Songlin Liu [a], Chunyi Xie [a]

[a] Institute of Plasma Physics, Chinese Academy of Sciences, Hefei, China
[b] ITER Organization, Route de Vinon Sur Verdon, Saint Lez Druance, France
[c] Institute of Energy and Climate Research – Plasma Physics, Forschungszentrum Jülich GmbH, Association EURATOM-FZJ, Jülich, Germany
[d] Sandia National Laboratories, Albuquerque, NM, USA
[e] University of Toronto Institute for Aerospace Studies, Toronto, Canada
[f] National Institute for Fusion Science, Toki, Japan
[g] Japan Atomic Energy Agency, Naka, Ibaraki, Japan
[h] Kyushu University, Fukuoka, Japan

ARTICLE INFO

Article history:
Available online 30 September 2014

ABSTRACT

The Material and Plasma Evaluation System (MAPES) in the EAST tokamak has been built up and used to address a variety of plasma–material interaction (PMI) issues relevant to ITER in 2012 EAST campaign. The topics studied cover erosion/redeposition of plasma-facing materials and components, hydrogenic retention in the gaps of castellation structure, deterioration of diagnostic mirrors from impurity deposition and protective technique. An introduction of MAPES system and an overview of the recent experimental results are presented.

1. Introduction

PMI is one of the main aspects to be considered toward International Thermonuclear Experimental Reactor (ITER) and a future fusion reactor [1]. The interactions between the edge plasma and the surrounding material surfaces profoundly influences the conditions in the core plasma, thus affects tokamak operation in many ways. Erosion by the plasma determines the lifetime of plasma-facing components (PFCs) and creates a source of impurities, which can cool and dilute the plasma. Deposition of material onto PFCs alters their surface composition and can lead to long term accumulation of large in-vessel tritium inventories [2]. Retention and recycling of hydrogen from PFCs affect fuelling efficiency, plasma density control and the density of neutral hydrogen in the plasma boundary, which impacts particle and energy transport. Maintaining PMI at an acceptable level is a serious challenge for the next generation of fusion devices. In ITER, Particle and energy fluxes incident on the PFCs will have fluences orders of magnitude higher than those in contemporary machines, resulting in much higher erosion than presently observed [1]. Another problem related to erosion/re-deposition is deterioration of diagnostic mirrors that will be used by a majority of ITER optical diagnostics as a plasma-viewing element [3]. Deposition of carbon and/or beryllium on the mirrors may shut down the diagnostics working in the ultraviolet and visible wavelength ranges. Deposition mitigation and mirror cleaning techniques need to be developed.

2. MAPES system in EAST

The Experimental Advanced Superconducting Tokamak (EAST) is the world's first fully superconducting magnetic confinement facility with ITER-like magnetic field configurations and heating schemes. The mission of EAST is to demonstrate high power, long pulse plasma operations with plasma current $I_p \leqslant 1$ MA, toroidal field $B_T \leqslant 3.5$ T, and envisioned plasma pulse length up to 1000 s, thus providing an important platform to address physics and engineering issues for the nextstep high power long pulse fusion devices such as ITER and beyond. In 2012 campaign EAST has achieved high confinement H-mode plasma over 30 s with predominantly lower hybrid current drive (LHCD) and advanced

* Corresponding author at: 350 Shushanhu Road, P.O. Box 1126, Hefei, Anhui 230031, China.
E-mail address: gnluo@ipp.ac.cn (G.-N. Luo).

http://dx.doi.org/10.1016/j.jnucmat.2014.09.017
0022-3115/

lithium wall conditioning [4]. The long-pulse H-modes in EAST exhibit a confinement quality between type-I and type-III ELMy H-modes, with $H_{98(y,2)} \sim 0.9$, similar to type-II ELMy H-modes [5]. Li wall conditioning has proven to be an effective method employed in EAST to control hydrogenic recycling, lowering the recycling coefficient with fresh Li coating [6]. However, Li also brings a major impact on PMI study in EAST.

The actively-cooled ITER-like W/Cu divertor project has been launched at Institute of Plasma Physics, Chinese Academy of Sciences in 2011. As a transition phase (2011–2012), the first wall of EAST was installed with molybdenum tiles bolted to an actively cooled Cu heat sink, allowing for a steady-state heat load of 2 MW/m^2 and graphite tiles were used for the divertor region. In 2014 campaign, EAST further upgraded its upper divertor to ITER-like actively-cooled monoblock W/Cu-PFC. In the future, EAST will eventually become a full-W PFC machine [7].

The MAPES project was initiated in 2010, and aims to provide a comprehensive and flexible experiment platform not only for PMI research [8] but also for the test of big engineering components in real tokamak environments, such as plasma-facing material and component (PFMC) mock-ups, test blanket modules (TBM), flowing liquid lithium limiters (FLiLi Limiter). Furthermore, some dedicated diagnostic (e.g. the spectroscopic system to measure deposition of radio frequency waves in front of the low hybrid antennas) can also be supported on MAPES. The MAPES system is located at the mid-plane outboard H port of EAST and has a total length of about 7 m as shown in Fig. 1. A gate valve with a nominal diameter of 500 mm is directly connected to the H port, followed in sequence by sample exchange chamber, supporting frame with a 5.5 m bellow and 2.8 m guide screw, feedthrough port (for data, cooling water, puffing gas, heating current, etc.), and step motor for driving the movement of sample manipulator. The maximum weight of sample load is 20 kg, and to be upgraded up to 30 kg by adopting a kind of slide rail to support the manipulator in the mid-plane port instead of original single roller support. Multiple test samples can be loaded simultaneously on MAPES for plasma exposure only if the samples do not exceed the above space and weight limits. The sample on manipulator can be transported from the low field side to the main SOL region in EAST with an adjustable speed of 1–15 mm/s by either manually controlled or programmed controlling the step motor. Ultimately, the sample can be inserted to the position of 2.29 m in main radius, i.e. the normal separatrix, with a positioning precision of 0.5 mm.

MAPES is also equipped with sample water cooling and heating facilities to provide limited sample temperature adjustment depending on experiment conditions. A gas puffing component will be added for impurity transport studies in the next campaign. An independent vacuum pumping system is installed to evacuate the sample exchange chamber before connecting to the EAST main vacuum vessel, so that MAPES can be used to carry out a series of experiments with different samples without disturbing routine EAST operation and the Li wall conditioning impact on PMI study on MAPES can be diminished by choosing suitable plasmas. It would normally take 6 h for once sample exchange including sample installation and vacuum pumping, which could vary with different samples.

Several PMI diagnostics have been installed to observe PMI processes at the MAPES samples (Fig. 2). A Langmuir probe array embedded in samples and a dedicated optical emission spectroscopy system provide information on local background plasma and impurity. The temperature profile on the sample surface can be monitored by infrared camera at M sector and embedded thermocouples. The CCD camera at D mid-plane port can be used to observe the exposure processes on the sample surface in real time. The temporal and spatial resolutions are 20 ms, 7 mm at MAPES head for infrared camera system in the wavelength range of 7.5–13 μm and 10 ms, 8 mm for CCD camera system in the wavelength range of 380–780 nm. In 2012, MAPES was applied for the first time in EAST experimental campaign to address a series of PMI experiments relevant to ITER.

3. ITER migration tile experiment

ITER will operate long pulse, high performance and high fluence discharges near double null configuration with a close-fitting, almost plasma conformal wall. ITER design incorporates beryllium tile cladding of the main chamber walls and a tungsten divertor [9–11]. As a low Z material, beryllium has a low physical sputtering threshold and high erosion rate. In long pulse, high performance, steady state plasma regimes, beryllium eroded from first-wall panels (FWPs) especially near the secondary X-point region at the top of the main chamber may be too high and redeposit along with tritium. ITER FWPs will be shaped toroidally to protect leading edges and possible misalignments between adjacent panels from high heat loads. However this creates recessed regions shadowed from direct ion flux where eroded material and impurity may redeposit. Combination of low erosion threshold of beryllium, high particle fluence and FWP shaping structure could make the issue worse. Alternatively, material eroded from the first wall may deposit in the divertor. The location of deposition depends on the field configuration and plasma density. Tritium retained in deposited material will be harder to remove from FWP than from the divertor due to the lower first wall baking temperature (not exceeding 240 °C compared with 350 °C foreseen for the divertor). Excessive tritium retention could hinder ITER operation due to limits on the in-vessel tritium inventory and erosion may limit component lifetime.

ITER organization (IO) has used the LIM–DIVIMP Monte-Carlo impurity transport code to assess the magnitude and distribution of erosion and deposition on realistic FWP and background

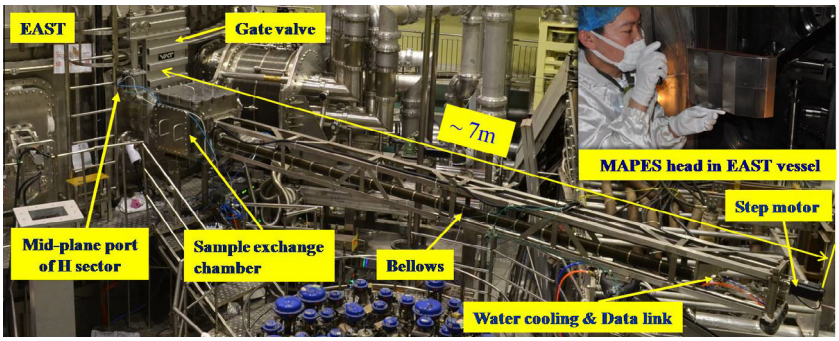

Fig. 1. Material and Plasma Evaluation System (MAPES) on EAST.

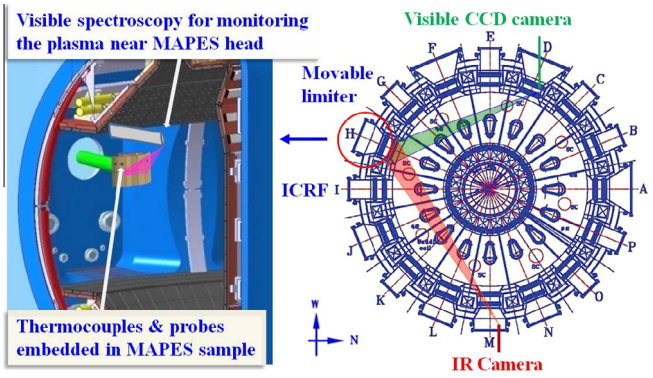

Fig. 2. PWI diagnostics available for MAPES head.

plasmas and hence the potential impact of these processes on ITER operation [12]. The 3D ERO code has also been used to benchmark against the results of the LIM code and excellent agreement achieved when all inputs are matched [13]. The following controlled experimental benchmark for the limiter-like erosion–redeposition simulations (LIM and ERO) was carried out by MAPES in EAST to test these simulation efforts.

A scaled-down proxy for ITER FWP was designed as an 18.0 × 26.6 cm assembly of 12 flat Mo plates tiles shaped in the toroidal direction (Fig. 3). Four Langmuir probe (LPs) were flush mounted inside the flat plate sections of the tile and distributed symmetrically on two sides of the assembly tile divided by central vertical slot as shown in Fig. 3. The probe material is graphite with a diameter of 6 mm. This probe layout provides a small degree of radial resolution and also forms a 2-point Mach Probe profile in the SOL. The background flow is a further important constraint on the impurity transport modeling. Four thermocouples (TCs) were inserted into the tiles from the back side, 3 mm behind the front surface and 18 mm above the four LPs vertically, as indicated in Fig. 3. Two sets of identical proxy tiles were prepared for blank test and real exposure, respectively. Firstly, a set of uncoated Mo tiles was installed on MAPES head to sweep the edge plasma to establish an optimum experiment protocol. After any issues with the blank test had been resolved, the real experiment with a coated final version of the migration tile on the MAPES head was performed. Helium plasma discharges were used to eliminate carbon

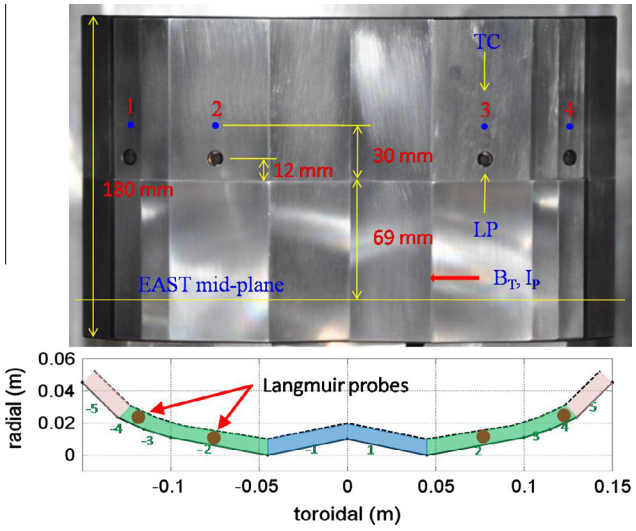

Fig. 3. Photo of front view (above) and diagram of poloidal view (below) of the ITER migration tile assembly.

chemical erosion as on the carbon coated tiles because the erosion channel does not exist for Be. Another consideration is that He plasmas are cleaner than their deuterium counterparts in a machine containing carbon, such as EAST with carbon divertors in the 2012 campaign. Ohmic double null divertor discharges were chosen so that no complicating features like ELMs or low hybrid heating would make the SOL plasma more difficult to understand and for better plasma shaping. To avoid direct contact of the start-up and ramp-down plasmas with samples, high field side (HFS) ramp-up/ramp-down was used, so that the samples were exposed only to the flat top diverted plasma phases.

In the blank test, the MAPES head with uncoated Mo tiles was moved progressively inwards in a series of successive identical shots similar to those in the photos of Fig. 4 acquired by the camera at mid-plane port D. Fig. 5 displays the major parameters in the successive He discharge shots 44,162–44,166 with varying MAPES head positions from 2.285 m to 2.325 m in main radius. The CXUV data show a rise of core radiation with the MAPES head moving in and eventual disruption with MAPES just inside the nominal separatrix (shot 44,162). In these shots outboard start-up limiters were fixed at 2.345 m and the separatrix kept at 2.29 m in main radius with an error within 5 mm. The edge plasma parameter profiles in the blank test shots were obtained from the embedded LPs and a fast reciprocating probe at mid-plane port F, respectively. After comparing the measured plasma profile with previous scoping simulations with LIM–DIVIMP [12], 2.315 m was considered as the optimum radial position for the migration tile, for which the simulation results predicted a moderate erosion of the carbon coating, i.e. neither beyond the detection limit nor completely eroding the 2 μm coating layer.

Before the second real experiment, a carbon layer as proxy for beryllium was deposited on the second set of Mo plates by magnetron sputter deposition at Sandia National Laboratory (SNL). Prior to exposure the C thickness was measured with Rutherford backscattering spectrometry (RBS) at 72 locations. The mean thickness is 1.92 ± 0.12 μm [14]. The coated migration tiles at 2.315 m in main radius were exposed to the flat top plasmas of 16 subsequent identical EAST shots 44,179–44,195 with the optimum conditions, i.e. ohmic L-mode, double null divertor, He discharge with a plasma current of 400 kA and toroidal magnetic field of 2.0 *T*. The central line-averaged electron density and temperature were 1.6×10^{19} m^{-3} and 0.6 keV respectively. Each shot has a 6 s flat top plasma, so the total exposure duration is 96 s including a disrupted shot 44,193 which broke down at 0.6 s in ramp-up phase. The reconstructed magnetic equilibrium by EFIT code shows that the plasma column in shot 44,193 was near high field side and had a downward moving tendency before the disruption. Moreover, the runaway electrons, which are often produced at disruption and cause the erosion or melting of PFCs, are believed to be negligible for $B_T \leqslant 2.2$ *T* [15]. So the influence of this disrupted shot on tile erosion could be neglected. Fig. 6(a) and (b) present time traces of ion saturation flow and surface temperature obtained respectively by LPs and TCs embedded in the tiles in shot 44,185. The embedded LPs show that there is a strong ion-side/electron-side ion flux asymmetry on the tile surface. Ion/electron side refers to the directions from which ion or electron drift flux impinges onto the probes due to the plasma current, indicated by I_p in Figs. 3 and 4. The typical electron temperature and density are 12.8 eV, 1.0×10^{18} m^{-3} at LP2 and 13.2 eV, 1.9×10^{18} m^{-3} at LP3. A similar asymmetry was also found in the temperature distribution on the tile surface recorded by IR camera [14] and embedded thermocouples (TC) (Fig. 6(b)). More particle flux and heat flux were present at ion-side compared with those at electron-side. Moreover, the off-midplane position produces heavier loading on lower side of migration tile and adds to the i-side/e-side asymmetry [14].

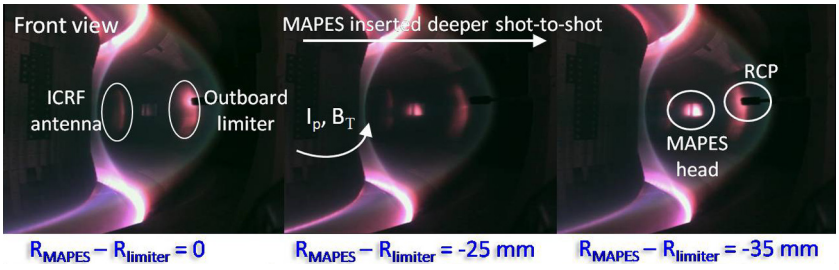

Fig. 4. Photos of MAPES head exposed to a serial of identical discharge plasmas with progressively deeper positions. The outboard limiter at G mid-plane port was fixed at 2.345 m and the seperatrix at 2.29 m in main radius. D plasma was applied in these tests.

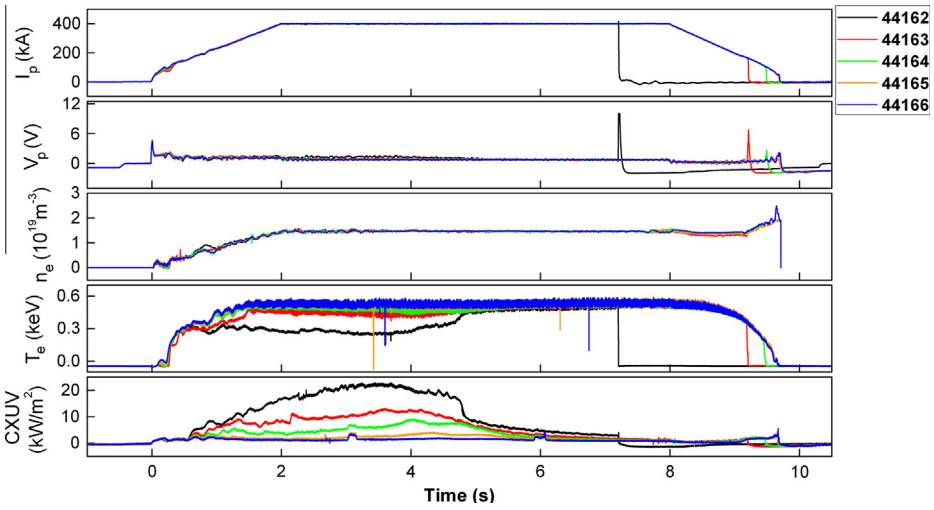

Fig. 5. Time traces of the main shots parameters in the series of blank tests of He discharges. MAPES head moved out from plasma with the same step from shot 44162–44166.

The erosion–deposition pattern on the migration tile was obtained by measuring the carbon thickness again at the same 72 locations after plasma exposure [14]. The results show that the plasma exposure produced a peak erosion of about 800 nm at a rate of 8 nm/s, near the midplane on the side facing the ion-drift direction. Erosion on the electron-drift side is about a factor of two lower than on the ion-drift side at the same poloidal position and erosion decreases from 6.5×10^{18} atoms/cm^2 to 0.5×10^{18} atoms/cm^2 with increasing poloidal position. The surface analysis results are consistent with the particle flux and surface heat flux asymmetry indicated by the LP, TC data and the IR image. No net local deposition was observed with a detection limit of 40 nm. Simulations of these results and underlying mechanisms will be discussed in a subsequent paper. This experiment demonstrates the feasibility of MAPES providing data needed to benchmark codes for the simulation prediction of erosion/deposition in ITER FWP. However, the shadowing effect of neighboring components could change the connection lengths and affect the particle flow in the SOL region, thus complicate the interpretation of the experiment results. The influence of the ICRH limiter at I port and the outboard limiter at G port should be evaded in the future. In addition, the magnetic field pitch angle on MAPES head is also a critical factor and should be considered for the optimization of the experiment scenarios.

Due to the lack of local or global measurement of the purity of He plasma on EAST, there could be an uncertainty of possible chemical erosion contribution of residual D in the He plasma flux to the erosion pattern. However, there were successive 47 He test shots before the exposure of C-coated tiles, so that the residual D concentration should be low according to the previous He discharges on JET [16]. In addition, He^3 Nuclear Reaction Analysis (NRA) measurement in SNL indicated that the areal density of D on the tiles was $1–2 \times 10^{16}$ atoms/cm^2, about an order of magnitude lower than is typically found on carbon surfaces undergoing net erosion by a D plasma which is $1–3 \times 10^{17}$ atoms/cm2 [17]. Z_{eff} in these plasmas was around 3 calculated based on the visible bremsstrahlung measure [18]. So the estimation of 10% D concentration in He plasma might be reasonable, which seems not to significantly change the ERO simulation results based on the chemical erosion yields calculated according to the Roth formula [19].

4. Investigations of tungsten castellated structures

The PFCs in ITER will be castellated to reduce thermal stress and induced eddy current loops. Radioactive fuel accumulation in the gaps of castellated structures may be a potential safety issue [20]. Preceding work shows that the impurity deposition and associated deuterium inventory in shaped gaps could be reduced compared with that in rectangular ones [21]. After the TEXTOR team finalized the predictive modeling assessment of an envisaged optimized castellation, a multi-machine joint experimental validation in order to qualify the optimized geometry was planned within the IEA–ITPA Joint Experiments program, task DSOL 27.

ITER-grade tungsten castellation structures (Fig. 7) supplied by Forschungszentrum Jülich (FZJ) were exposed to EAST plasmas in a piggyback mode over two days using MAPES. Fixed at a radial position of 2.376 m, 10 mm behind the adjacent outboard limiter at G port, the castellation samples were exposed to 12 L-mode discharges (43,333–44, 1000 s) with a line-averaged electron density of 1×10^{19} m^{-3} and 73 H-mode discharges (43,351–423, 400 s)

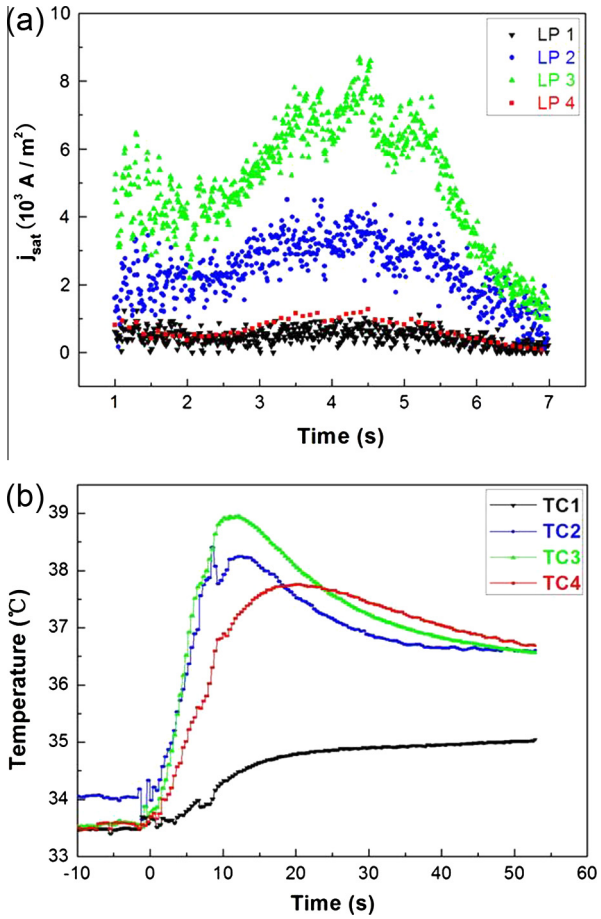

Fig. 6. Time traces of the ion saturation flow (a) and the surface temperature (b) obtained respectively by Langmuir probes and thermocouples embedded in the ITER migration tiles in shot 44,185, showing a strong ion-side/electron-side ion flux and temperature asymmetry on the tile surface. Larger particle flux and heat flux were found at ion-side.

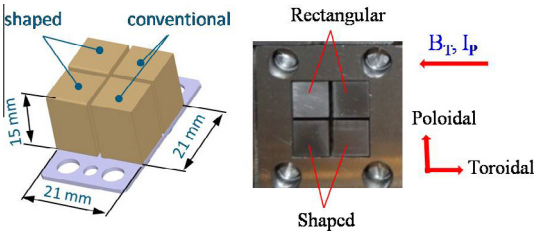

Fig. 7. Diagram (left) and photo (right) of the identical ITER-grade tungsten castellation structures.

with varying densities of 2–5 $\times$ 10^{19} m^{-3}. The embedded LPs indicated that typical flux to the castellation sample was around 2 $\times$ 10^{21} m^2/s. During these discharges, the ICRF antenna at I port was withdrawn outwards and the surface temperature increase was no more than 60 °C indicated by the embedded TCs.

After the exposure, the castellation samples were delivered to FZJ for analysis of the deposits. The top plasma-wetted tungsten surfaces were still metallically shiny, and the deposition patterns at the side surfaces of poloidal gap were measured by electron-probe micro-analysis (EPMA). Fig. 8 exhibits the deposition profiles of carbon on the sides of the gaps. For the non-shaped cell the deposition pattern is much more peaked at the plasma-closest edge of the gap with higher maximum value than that for shaped cell. The deposition profiles were integrated for both

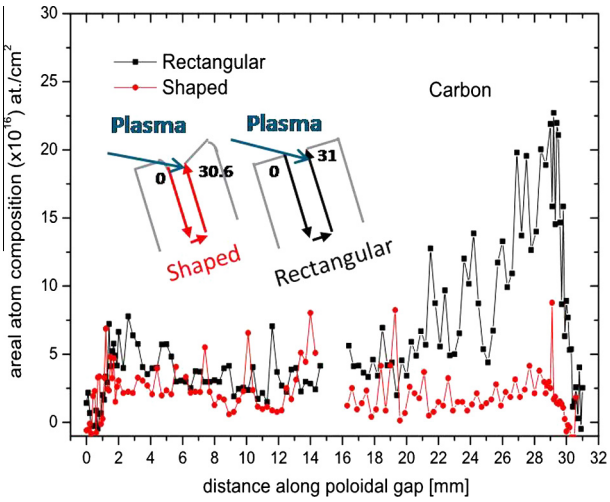

Fig. 8. Deposition profiles of carbon on the sides of gap measured by EPMA after exposure.

geometries of cells in order to get the total amount of carbon in the gaps. Significantly lower amounts of carbon (6.5 $\times$ 10^{17} atoms) were found in the deposits of shaped cells, compared with those (1.7 $\times$ 10^{18} C atoms) of rectangular ones, confirming the predicted advantage of shaping optimization for the reduction of impurity deposition in the gaps. However, what puzzles us is that more C deposits were found on the plasma-open side than those on the plasma-shadowed side in rectangular cell, which is just the reverse of previous results [21,22]. The shaping effects on the mitigation of impurity deposition are also more pronounced on the plasma-open side. This could imply that important physics processes are still missing in the predictive modeling. In this exposure case, the magnetic field line was almost parallel to the castellation surface, different from previous oblique cases in other devices [21].

There was a second set of castellations exposed, as a piggyback experiment, to a series discharges with varying scenarios for other experiment proposals. In these discharges the castellation sample was placed in a reversed direction with respect to the toroidal field direction at 2.349 m main radius, 4 mm behind both the main limiter at G port and the ICRF antenna at I port. No obvious difference in deposition patterns for rectangular and shaped cells was observed. The reason could be related to the complex SOL flow partly due to the similar connection lengths from castellation to limiter and ICRF antenna at adjacent ports and exposure almost parallel to the magnetic field. An improved experiment scenario is being planned for the exposure in next EAST campaign including inclination of the castellation to the magnetic field, longer exposure duration and closer position to the plasma.

5. Exposure of first mirror with protective duct

Optical mirrors are foreseen to be applied widely in ITER diagnostics, and they will work in infrared, visible and ultraviolet wavelength ranges. Mo, W and stainless steel are among the main candidate mirror materials to be used in ITER. However, the optical property of mirrors will deteriorate due to erosion, deposition of non-volatile impurity species and particle implantation [23]. The effectiveness of protective ducts on the optical properties of first mirrors was investigated using MAPES (Fig. 9), by exposing a set of Mo mirrors with ducts of different lengths.

Facing the main plasma, the first mirror (FM) array (Fig. 9(a)) was vertically fixed at 2.385 m main radius, 40 mm behind the

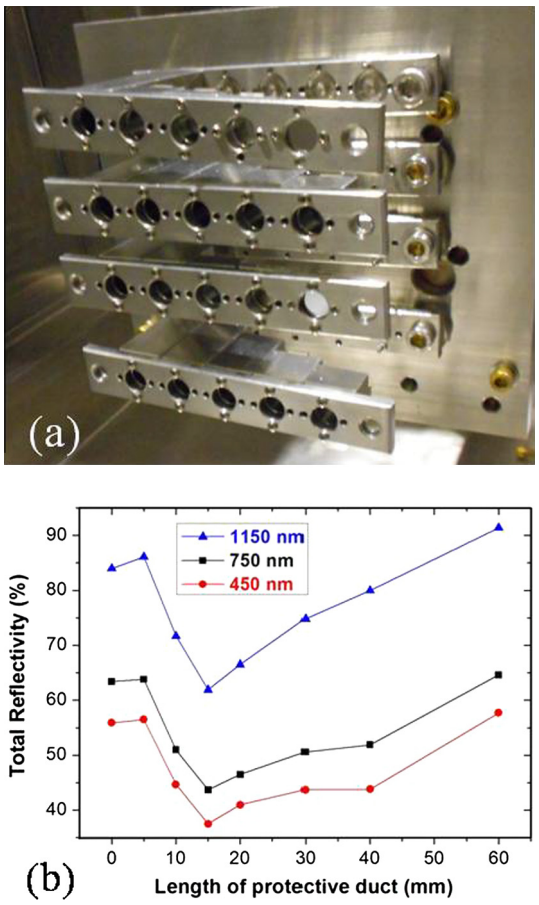

Fig. 9. (a) Mo first mirror array on MAPES head. (b) Dependency of the reflectivity of exposed Mo mirror at three wavelengths of 450 nm, 750 nm and 1150 nm on the protective duct lengths from 0 mm to 60 mm. The reflectivity of unexposed Mo mirror is 58% at 450 nm, 65% at 750 nm, and 92% at 1150 nm, respectively.

main limiter at port G, i.e. 95 mm from the separatrix. The line-averaged D plasma density ranged from 2–3 $\times$ 10^{19} m^{-3} during the exposure. Plasma parameters near the samples could not be measured due to the low signal to noise ratio of the embedded probe's signals. The total exposure duration was 3000 s in 176 shots. Fig. 9(b) presents the dependency of FM total reflectivity at three wavelengths (450 nm, 750 nm and 1150 nm) on the length of the protective duct after exposure. The three plots present the similar trend. There is a first drop in reflectivity followed by a rise with increasing duct length. The shortest three ducts show an opposite trend to those longer than 10 mm. The FM without protective duct keeps almost the same reflectivity as the unexposed one and the one with a 60 mm duct.

The impinging particle flux on FM ducts could be around 10^{21} m^2/s estimated from other probe data. The TC data showed that the temperature in that region was normally no higher than 50 °C. The surface temperature differences at the different mirror positions should be within 20 °C. So the temperature effect could be negligible. The plasma erosion effect should be considered here. The variation of reflectivity with increasing duct length could arise from a net result of erosion and deposition processes, i.e. the influence of deposition was offset by erosion due to ion impact on the surface, which is similar to the results in JET [24]. For the first two positions, significant re-erosion took place to better the balance of erosion to deposition. With an initial increase of duct length, the transport of charged particles into the duct would be dampened more rapidly than that of neutral particles, leading to a net deposition on FM and corresponding deterioration of reflectivity. With a longer duct, fewer neutrals could reach the FM surface and the reflectivity was improved as shown in Fig. 9(b).

6. Summary and future plan

A Material and Plasma Evaluation System with sample load capability up to 20 kg has been developed on EAST. A range of ITER-relevant PMI experiments have been successfully conducted in EAST tokamak employing MAPES. Dedicated migration experiments were carried out and provided integrated plasma surface erosion and deposition data needed to benchmark codes being used to predict erosion/deposition at ITER FWPs. A new proposed shape of divertor W-castellations was experimentally tested using MAPES. The performances of conventional and optimized shapes were compared. A factor of 2.5 less carbon were found in the gaps of shaped poloidal cells compared with non-shaped ones. The obtained deposition patterns in gap samples will be used for code validation. The effectiveness of protective ducts on the optical properties of first mirrors was investigated using MAPES by exposing Mo mirrors with different lengths of productive ducts. After exposure in the erosion-dominated region, the FMs showed an initial decrease followed by increasing reflectivity with increasing duct length. The balance of erosion to deposition might pay an important role in the variation of FM reflectivity after exposure.

Several points still need to be optimized for the MAPES in the future. The MAPES head should be positioned in an oblique angle to the toroidal field, so that the plasma background during exposure could be closer to ITER conditions. The shadowing effects by neighboring PFCs should be avoided. A simpler boundary plasma background will make the experiment results easier to be analyzed.

Some new facilities are being developed on the MAPES, including the dedicated visual spectroscopy system for monitoring the plasma near MAPES head, and the gas puffing system for future impurity transport research on the MAPES. With more flexibility, MAPES application will be extended to wider fusion research scopes in next EAST campaign, including liquid Li loop system test, spectroscopic measure of the deposition of RF Waves in front of low hybrid antennas, TBM mockup experiment to study RAFM (reduced activation ferritic/martensitic) steel ripple effect on plasma [25]. As a versatile system, MAPES will not only continue to be applied to the studies of PMI issues, but also extended to the exploration of other physics and engineering issues related to ITER and future DEMO.

Acknowledgments

This work was supported by the National Magnetic Confinement Fusion Science Program of China under Contracts Nos. 2011GB110003, 2013GB105001, 2013GB105002, 2013GB105003 and 2013GB107004, the National Natural Science Foundation of China (NSFC) with Grant Nos. 11205198, 11075186, 11105180, 11375010 and 11305213, as well as the Joint Sino-Germany research project GZ765. The views and opinions expressed herein do not necessarily reflect those of the ITER Organization.

References

[1] G. Federici et al., Nucl. Fusion 41 (2001) 1967.
[2] S. Brezinsek et al., Nucl. Fusion 53 (2013) 083023.
[3] A. Litnovsky et al., Nucl. Fusion 47 (2007) 833.
[4] J.G. Li et al., Nat. Phys. 9 (2013) 817.
[5] H.Y. Guo et al., Nucl. Fusion 54 (2014) 013002.
[6] G.Z. Zuo et al., J. Nucl. Mater. S90 (2013) 438.
[7] G.-N. Luo et al., Fusion Sci. Technol. 62 (2012) 9.
[8] C.P.C. Wong et al., J. Nucl. Mater. 363–365 (2007) 276.
[9] G. Federici et al., Phys. Scr. T124 (2006) 1.
[10] R.A. Pitts et al., Phys. Scr. T138 (2009) 014001.

[11] R.A. Pitts et al., J. Nucl. Mater. 415 (2011) S957. ITER STAC-15 meeting.
[12] S. Carpentier et al., J. Nucl. Mater. 415 (2011) S165.
[13] D. Borodin et al., Phys. Scr. T145 (2011) 014008.
[14] W.R. Wampler et al., Phys. Scr. T159 (2014) 014069.
[15] R. Yoshino, Nucl. Fusion 39 (1999) 151.
[16] R.A. Pitts et al., J. Nucl. Mater. 313–316 (2003) 777.
[17] W.R. Wampler et al., J. Nucl. Mater. 337–339 (2005) 134.
[18] Y.J. Chen et al., Fusion Eng. Des. 88 (2013) 2825.
[19] J. Roth et al., J. Nucl. Mater. 266–269 (1999) 51.
[20] K. Krieger et al., J. Nucl. Mater. 363–365 (2007) 870.
[21] A. Litnovsky et al., J. Nucl. Mater. 390–391 (2009) 556.
[22] A. Litnovsky et al., J. Nucl. Mater. 415 (2011) S289.
[23] A. Litnovsky et al., J. Nucl. Mater. 417 (2011) 830.
[24] D. Ivanova et al., Phys. Scr. T159 (2014) 014011.
[25] S.L. Liu, et al., in: Proceedings of the 21st International Conference on Nuclear Engineering, Chengdu, China, 2013.